Environ. Sci. Technol. **1998**, *32,* 3743−3748

Reactivity of the (100) Plane of Pyrite in Oxidizing Gaseous and Aqueous Environments: Effects of Surface Imperfections

JEFFREY M. GUEVREMONT,[†] JOAKIM BEBIE,[‡] ALICIA R. ELSETINOW,[†] DANIEL R. STRONGIN,*[,†] AND MARTIN A. A. SCHOONEN[‡]

Department of Chemistry, Temple University, Philadelphia, Pennsylvania 19122, and Department of Earth and Space Sciences, State University of New York, Stony Brook, New York 11974-2100

The oxidation-induced degradation of pyrite in mine tailing piles is of significant interest, since the resulting production of sulfuric acid has a severe detrimental impact on the surrounding environment. Hence, there has been much effort to understand the mechanism of pyrite oxidation. Much of the information concerned with the surface reactivity of pyrite, however, has been inferred from macroscopic observations during aqueous studies. Here, we directly investigated model FeS_2(100) surfaces after exposure to well-defined oxidizing environments, with X-ray photoelectron spectroscopy, to evaluate the mechanism of pyrite oxidation at a microscopic level. Our studies showed that, in the pure H_2O vapor environment, oxidation of FeS_2-(100) was spatially limited to nonstoichiometric or sulfur-deficient surface sites. Results further suggested that thiosulfate was a long-lived intermediate that ultimately converted to sulfate on the pyrite surface in this environment. Significant oxidation of the disulfide group of FeS_2(100) only occurred if O_2 was present along with H_2O vapor (O_2 alone resulted in only minor reaction). It is proposed that O_2 adsorption on the stoichiometric region of FeS_2-(100) resulted in the formation of Fe^{3+} sites that facilitated the dissociation of H_2O and the oxidation of the disulfide group.

Introduction

There is significant interest in understanding the oxidation of pyrite, because it is the root cause for acidification of streams draining coal and metal−sulfide mines. Mine waste from coal mines and metal−sulfide mines is often rich in pyrite, and weathering leads to the production of large amounts of sulfuric acid. The extremely acidic runoff, often referred to as 'acid mine drainage', is a considerable environmental concern (*1*), and methods are sought to reduce the rate of pyrite oxidation. Effective methods can only be developed if the mechanism of pyrite oxidation is understood at the molecular level.

Pyrite oxidation has been investigated in numerous aqueous studies in which rate laws were established. For recent reviews on sulfide mineral oxidation, see Alpers and Blowes (*2*), Nordstrom and Southam (*3*), and Williamson and Rimstidt (*4*). Reaction mechanisms are often proposed on the basis of rate data obtained in aqueous studies (*5*−*7*). The effects of pH, dissolved oxygen, and Fe^{3+} on oxidation rates have been investigated (*8, 9*). However, aqueous studies do not yield molecular level information relating to the surface composition and the effects of surface structural imperfections on the surface reactivity of pyrite. Hence, there is a need for observations at the molecular level to corroborate the proposed reaction mechanisms.

Ultrahigh vacuum (UHV) spectroscopic techniques have been used in prior works to gain insight into the atomic level surface structure and reactivity of pyrite (*10, 11*). Exposure of the pyrite surfaces to water and/or molecular oxygen has been achieved via a number of methods, ranging from careful dosing in the UHV experimental apparatus to exposure for prolonged periods of time to uncontrolled ambient conditions (*12*−*17*). Our study was built on these prior seminal works and investigated the (100) face of pyrite with vacuum-based electron spectroscopies after exposure to gases and aqueous solutions of known composition under a controlled atmosphere. The transfer of the sample between the vacuum and gaseous/liquid environments was carried out without exposure to the ambient. In contrast to the prior vacuum-based research, our studies have started to directly determine the chemical transformations that occur on the pyrite surface after exposure to well controlled and environmentally relevant H_2O and H_2O/O_2 environments. Furthermore, results from these studies have emphasized the importance of nonstoichiometric regions of pyrite, which appear to be an inherent part of this mineral surface, in controlling some of the aspects of pyrite oxidation.

Experimental Section

All the electron spectroscopic data presented in this paper were obtained in a stainless steel ultrahigh vacuum (UHV) chamber with a working base pressure of 1×10^{-9} Torr. UHV was obtained by use of cryogenic helium refrigerator and turbomolecular pumps. The chamber was equipped with a double-pass cylindrical mirror analyzer (CMA), X-ray source, and ion gun for sample cleaning. An important feature of this apparatus was a sample transfer device (*18*). In short, the sample could be removed from the UHV chamber into an intermediate vacuum chamber (pumped by turbomolecular pump) and then transferred in an inert N_2 atmosphere to a reaction cell where liquid and vapor dosing were carried out.

Pyrite used in this research was obtained from Longrono, Spain. Samples from which data were obtained were all approximately 2 mm thick square plates with areas of ∼1 cm^2. One side of each plate was an as-grown surface, and the sample was handled carefully as to avoid any mechanical or chemical alteration of this natural surface outside the UHV chamber.

Pyrite samples were mounted individually on an UHV-compatible holder that allowed heating of the pyrite sample (temperature monitored by a K-type thermocouple). Preparation of an atomically clean FeS_2(100) sample for UHV studies was carried out by the same method that has been described in detail in an earlier publication (*19*). One adjustment to the procedure in this case was to sputter with 1000 eV He^+ to compensate for a rather poor ion bombardment geometry. The higher energy bombardment induced structural changes to the samples, but it was needed to remove the C and O contamination that was present on the

* To whom correspondence should be addressed. Telephone: (215)204-7119; fax: (215)204-1532; e-mail: dstrongi@nimbus.ocis.temple.edu.

[†] Temple University.

[‡] State University of New York.

10.1021/es980298h CCC: $15.00
Published on Web 10/15/1998

as-introduced sample. After UHV cleaning, the sample was transferred (see below) and cleaned in an atmospheric reaction cell by washing the surface with 0.5 M HCl. The sample was then reintroduced into UHV for analysis by X-ray photoelectron spectroscopy (XPS). Acid-washing the sample after UHV cleaning removed surface imperfections due to the ion bombardment cleaning step (*20*).

XPS was performed by using unmonochromatized Mg Kα radiation (1253.6 eV) as the excitation source. Binding energies of the S 2p, Fe 2p, and O 1s core levels were obtained by measuring the kinetic energy of the photoemitted electrons with an electron analyzer pass energy of 25 eV. XPS is an informative technique in this study since changes in the kinetic energy of photoemitted electrons from the atomic core levels of a particular element in the surface region of a solid are relatable to changes in its valence charge that occur during oxidation (*21*). In particular, the kinetic energy of the electrons photoemitted from the S 2p and Fe 2p levels after pyrite is reacted in oxidizing gaseous and liquid environments can be used to determine the postreaction oxidation states of those elements. XPS data, like many other spectroscopic techniques, require curve fitting analysis to extract some of the information. In the analysis of our data, the $2p_{3/2}$ and $2p_{1/2}$ contributions to each S 2p doublet used to fit spectral data in this contribution have been constrained by a 2:1 peak area ratio, 1.18 eV separation, and 1.3 eV full-width at half-maximum.

Aqueous solutions were prepared following the protocol outlined in Bebie et al. (*22*) in a glovebag. To deoxygenate solutions, they were purged for at least 2 h with high-purity nitrogen gas that was first passed through a sulfite oxygen trap (sulfite reacts quantitatively with molecular oxygen to form sulfate). Solutions were introduced into the reaction cell through a serum cap (separated the glovebag from the interior of the reaction cell) with a glass syringe with stainless steel needle. The sample was held at an angle to allow flow over the sample and into a drain. After exposure, the sample was blown dry with a stream of ultrapure N_2, then returned to the intermediate chamber, reattached to the UHV sample holder, and returned to the UHV chamber for spectroscopic study. XPS of reference samples of Na_2SO_4 and Na_2SO_3 were prepared by placing a droplet of 1 mmol solution of the particular species on a pyrite surface and letting it dry in a N_2 atmosphere in the reaction cell. These samples were sufficiently thick to suppress the majority of signal from the underlying pyrite surface. The relative S 2p and O 1s XPS cross sections were determined from these reference compounds. Vapor doses were carried out by introducing the liquid of interest directly into the closed reaction cell without contacting the sample. After exposure to gas or liquid, the sample could be returned to the UHV chamber for analysis in about 15 min.

Results

Exposure of Different FeS_2(100) Samples to H_2O Vapor. (a) Acid-Washed FeS_2(100). S 2p data for the acid-washed sample before exposure to H_2O were fitted with two doublets at 162.3 and 161.5 eV (Figure 1A). The former peak position was associated with S in the disulfide group of FeS_2, and the latter with S in a coexisting monosulfide species (*10, 13, 17*). Visual inspection of S 2p XPS data after H_2O exposure (Figure 1A) showed significant spectral differences relative to the clean acid-washed spectrum. The changes were emphasized by a difference spectrum (inset to Figure 1A), obtained by subtracting the acid-wash data from the 20-h H_2O exposure data. Specifically, spectral weight at 161.5 eV decreased, and weight increased at 168.6 and 163.4 eV. The S 2p spectrum of the surface exposed to H_2O vapor was fitted with doublets at these latter two binding energy positions. The absence of a feature near 162.3 eV in the difference plot emphasized

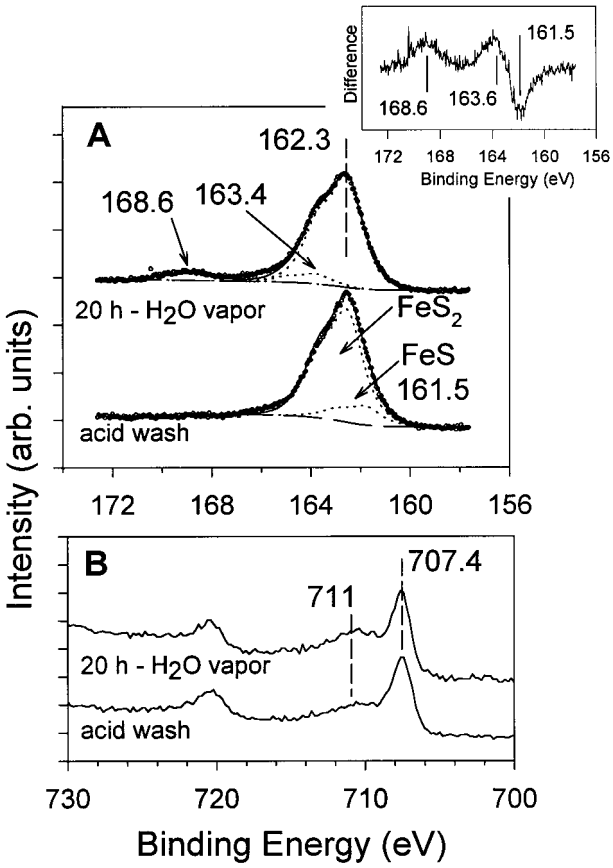

FIGURE 1. (A) S 2p data of acid-washed FeS_2(100) before and after exposure to 18 Torr of H_2O vapor for 20 h. Dashed curves are fitted S 2p doublets. (B) Fe 2p data for the same conditions.

that the disulfide group was largely unreactive in H_2O vapor. Analysis of the fitted curves showed that the ratio of the integrated intensities of the two doublets at 168.6 and 163.4 eV was 1.2 ± 0.3. Furthermore, the doublet at 161.5 eV present in the acid-washed spectrum was significantly reduced after exposure to H_2O vapor, suggesting that the majority of Fe−S was consumed and converted into S oxidation products under our experimental conditions.

Fe 2p data (Figure 1B) for acid-washed FeS_2(100) exhibited a main Fe $2p_{3/2}$ contribution at 707.4 eV that was associated with the iron component of pyrite (*13, 17*). The broad high energy tail on this feature was probably associated with some Fe^{3+} impurity. After exposure to H_2O vapor, there was no noticeable change in the pyrite−Fe peak at 707.4 eV and perhaps an increase in spectral intensity at 711 eV, suggesting that some oxidation of the iron component did occur.

(b) Partially Defective FeS_2(100). S 2p data associated with a pyrite surface that was ion bombarded for 2 h (no acid-wash afterward) showed an increase in monosulfide (spectral weight at 161.5 eV) in the near-surface region (Figure 2A). The increase in monosulfide was presumably due to the preferential removal of near-surface sulfur during ion bombardment. Exposure of this surface to 18 Torr of H_2O vapor (Figure 2A) eliminated the S 2p feature associated with Fe−S at 161.5 eV and resulted in the appearance of S 2p doublets at 168.6 and 163.4 eV. The S 2p doublet associated with the disulfide group of pyrite was unaffected during the exposure to H_2O vapor, within our experimental sensitivity.

Fe 2p data (Figure 2B) for FeS_2(100) that was acid-washed but which was subsequently ion bombarded showed excessive high energy spectral weight above ~710 eV. We suspect that the growth of spectral weight in this region was due in part to structural disorder and/or an increase in Fe^{3+} during

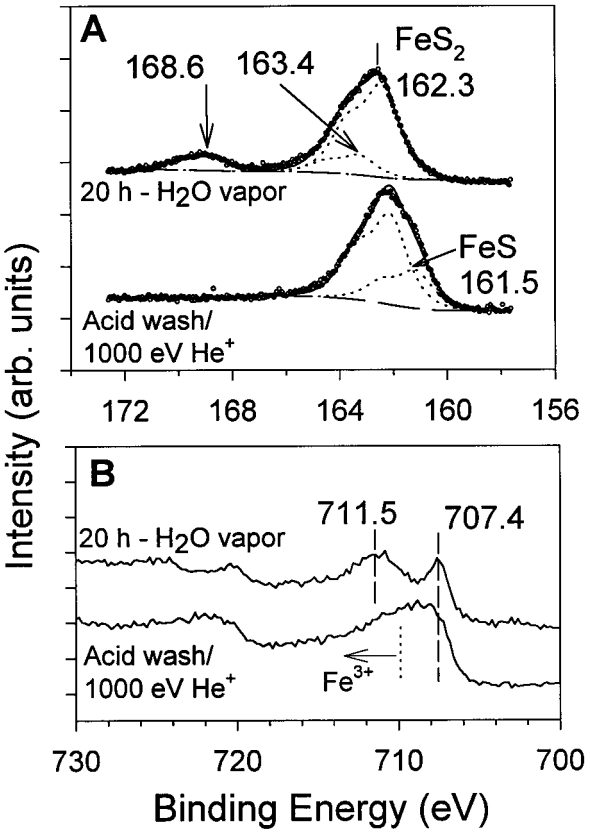

FIGURE 2. (A) S 2p data of acid-washed FeS_2(100), which has been ion bombarded to produce an enhanced amount of monosulfide defects, before and after exposure to 18 Torr of H_2O vapor for 20 h. (B) Fe 2p data for those conditions used to obtain the S 2p data.

ion bombardment. The broad high energy tail of the Fe $2p_{3/2}$ feature was largely removed upon exposure to H_2O vapor and in its place appeared two resolved features at 707.4 and 711 eV. The former feature was associated with pyrite−S. While the spectra was to broad to fit with confidence, we suspected that the 707.4 eV feature also contributed to the same extent in the S 2p spectrum obtained before H_2O vapor exposure. This contention was consistent with the S 2p data, which showed that the FeS_2 regions of the sample were unaffected by H_2O treatment. The 711.5 eV feature was assigned to Fe^{3+} species in an Fe−O product (such as an oxide, hydroxide, or oxyhydroxide).

(c) High Defect Density FeS_2(100). Highly defective FeS_2-(100) was prepared by a lengthy exposure to the ion beam after acid-washing. In this circumstance, the majority of the S 2p intensity (Figure 3A) was at a position that was associated with monosulfide. XPS analysis of this sample showed that the S 2p/Fe 3p peak area ratio was a factor of ~0.4 less than the analogous peak area ratio for the acid-washed sample that had not undergone ion bombardment. After a 20-h exposure, relatively well-defined S 2p features appeared at 168.6 and 163.4 eV. A further 100-h H_2O exposure resulted in a decrease in spectral intensity at 163.4 eV and an increase in intensity at 168.9 eV. Analysis of the fitted curves suggested that the S species associated with the 163.4 eV feature are converted into a sulfur oxide product associated with the 168.9 eV feature. Washing of the 100-h vapor exposure sample with deoxygenated H_2O liquid resulted in the elimination of the majority of the S 2p spectral weight at 168.9 eV. This spectral change was due to the dissolution of the sulfur oxide product into the liquid water.

O 1s data (Figure 3B) were obtained for the sample that had been exposed to 100 h of water vapor and after it has

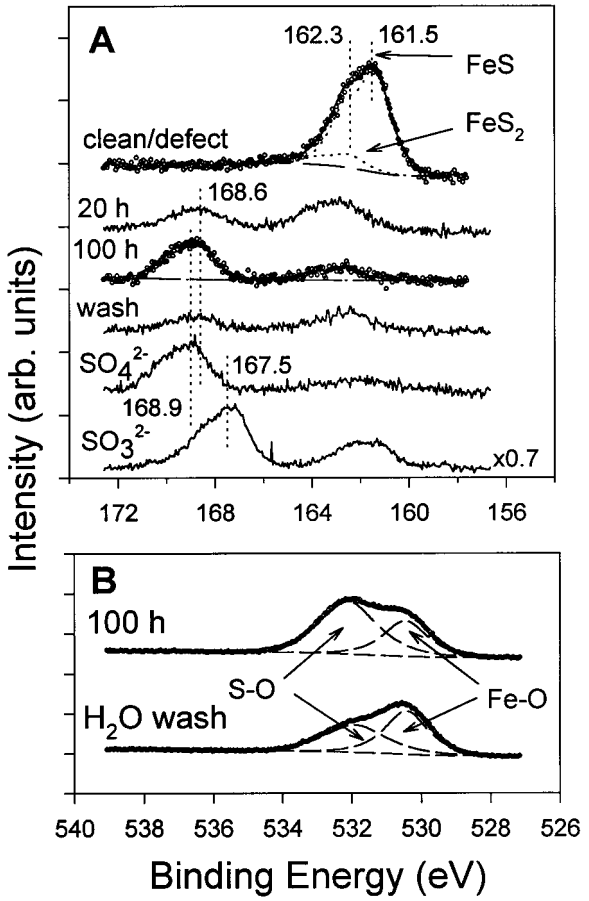

FIGURE 3. (A) S 2p data for a highly defective surface of FeS_2(100) after various treatments of H_2O vapor and liquid. Included in the S 2p panel are reference spectra for Na_2SO_4 and Na_2SO_3. (B) O 1s data for the highly defective FeS_2(100) after a 100-h exposure and after this surface is washed in liquid H_2O.

been washed in deoxygenated water. After the water wash, the spectral weight near 532 eV was largely removed, and this change was due to the removal of the sulfur oxide product. Prior XPS studies of sulfur oxide species on metal surfaces experimentally observed O bound to S to exhibit a O 1s binding energy near 532 eV (*23, 24*). The O 1s feature at 530.2 eV was attributed to an Fe−O product, and this contribution was relatively constant during the washing. By assuming that the loss of the S 2p and O 1s intensity (at 532 eV) was due to the dissolution of a single sulfur oxide product, it was estimated that the O:S stoichiometry of the sulfur oxidation product was 3.5 ± 0.4. Reference S 2p spectra for Na_2SO_4 and Na_2SO_3 were obtained to help product identification.

S 2p and O 1s data were obtained for the S product formed after the highly defective surface was exposed to water vapor for 20 h and after it was washed with deoxygenated water (Figure 4). Using the same procedure as mentioned above to determine stoichiometry, it was estimated that the O:S ratio of the product formed after a 20-h exposure was 1.3 ± 0.2. Furthermore the ratio of the 168.6 and 163.4 eV features associated with this product were close to unity (i.e., 1.2 ± 0.3). Both these observations pointed toward a product, such as thiosulfate (i.e., $S_2O_3^{2-}$). A reference spectrum of thiosulfate (see Experimental Section for preparation details) was obtained for comparison.

Exposure of FeS_2(100) to a H_2O/O_2 Gaseous Mixture. S 2p data (Figure 5A) after acid-washed FeS_2(100) was exposed to 20 h of O_2 suggested that less oxidation of the sulfur component occurred than in the pure H_2O vapor circum-

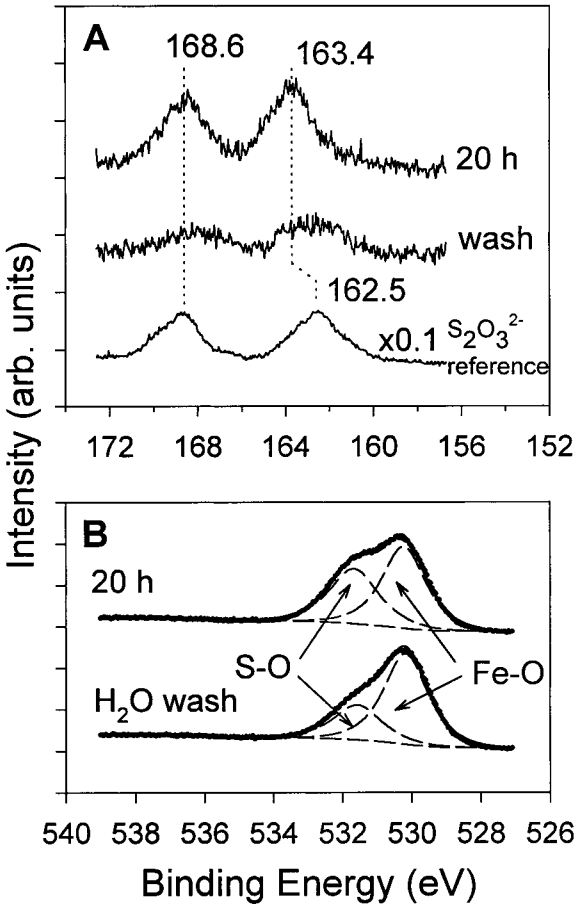

FIGURE 4. (A) S 2p data for a highly defective surface of FeS_2(100) after a 20-h exposure to H_2O vapor and after washing the reacted surface with deoxygenated H_2O. Also included in the S 2p panel is a reference spectrum of $Na_2S_2O_3$ obtained in our laboratory. (B) O 1s data obtained for those conditions used to acquire the S 2p data.

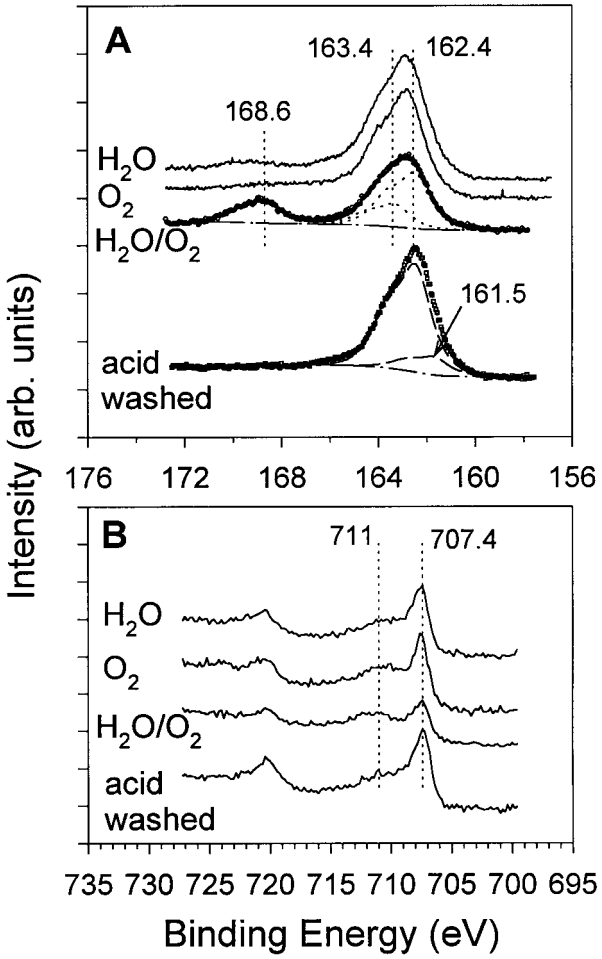

FIGURE 5. (A) S 2p data of acid-washed FeS_2(100) and after exposure to the indicated vapor environments. (B) Fe 2p data of acid-washed FeS_2(100) and after exposure to the indicated vapor environments.

stance. Exposure of acid-washed FeS_2(100) to a H_2O/O_2 mixture resulted in more substantial sulfur oxidation, as evidenced by relatively intense S 2p features at 168.6 and 163.4 eV. Furthermore, in contrast to pure H_2O or O_2 gas, the H_2O/O_2 mixture resulted in a significant oxidation of the disulfide group of FeS_2(100), based on the reduction of the 162.4 eV feature (relative to the analogous feature associated with the sample prior to exposure). Furthermore, the sum of the peak areas of the 168.6 and 163.4 eV features in the H_2O/O_2 spectrum were a factor of 2.1 greater than that of the 161.5 eV (monosulfide) in the acid-washed spectrum. Thus, the disulfide in addition to the monosulfide reacted in the H_2O/O_2 mixture.

Fe 2p data (Figure 5B) showed no noticeable changes after individual exposure to pure H_2O and O_2 [with respect to the Fe 2p spectrum associated with acid-washed FeS_2-(100)]. Spectral weight near 711.4 eV increased and intensity near 707.4 eV decreased after exposure to the H_2O/O_2 mixture, indicating significant oxidation of the iron component.

Surface Reactivity of FeS_2(100) in Aqueous Environments. A limited set of experiments were carried out that exposed acid-washed pyrite to deoxygenated H_2O, oxygenated H_2O, and deoxygenated H_2O with Fe^{3+}. No sulfur oxidation products were detected on the surface after evacuation of the liquid phase and reintroduction into the UHV chamber. This circumstance was due to the solubility of sulfur oxide product in the liquid phase, and hence, the S oxidation product could not be retained on the mineral surface for UHV analysis.

Significant changes in the Fe 2p and O 1s spectral lines (Figure 6, panels A and B, respectively), however, occurred in some cases after 1-h exposures to the different liquid environments. Exposure of FeS_2(100) to deoxygenated H_2O resulted in an Fe 2p spectrum that was, within our experimental resolution, largely indistinguishable from the clean spectrum. A greater amount of Fe oxidation occurred in oxygenated H_2O based on an increase of spectral weight near 711.5 (attributed to Fe^{3+} in an Fe−O product). More extensive oxidation occurred when acid-washed pyrite was exposed to ferric ion, and in this circumstance the entire population of Fe in the near-surface region became oxidized. O 1s data were consistent with the Fe 2p data in that the amount of surface oxygen was least in the case of deoxygenated water and greatest in the presence of aqueous Fe^{3+}. We did not attempt to analyze these spectra to determine the different O 1s contributions, since many species such as iron oxide, hydroxide, oxyhydroxide, or chemisorbed residual water might be expected to contribute to this O 1s region.

Discussion

Identification of Products Formed in the Oxidizing Environment. XPS cannot unambiguously identify surface reaction products on pyrite, but we present assignments that are most consistent with our data. There are two possibilities for the identity of the sulfur-derived product(s) after exposure of FeS_2(100) to H_2O vapor for 20 h. The S 2p spectrum for this circumstance might be interpreted as having contribu-

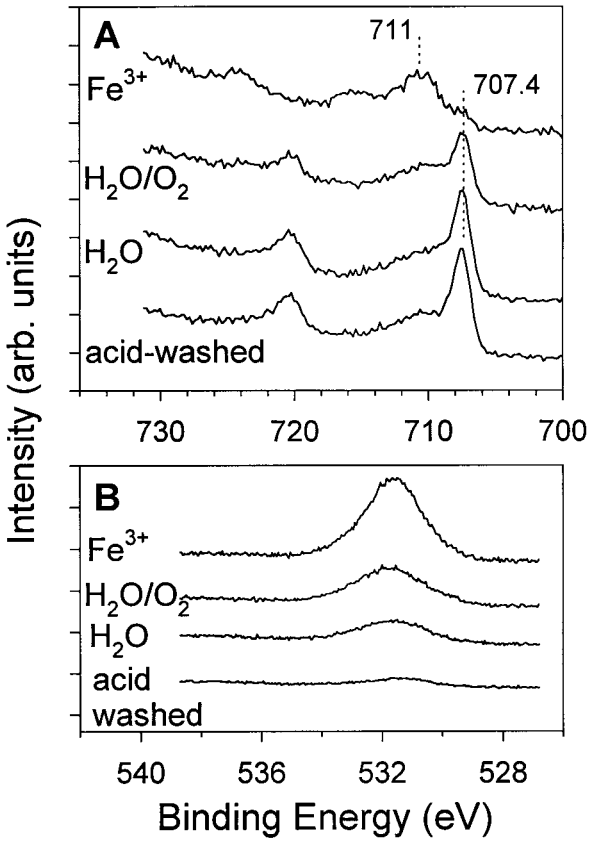

FIGURE 6. (A) Fe 2p data for acid-washed FeS_2(100) and after exposure to the indicated aqueous environments. (B) O 1s data for acid-washed FeS_2(100) and after exposure to the indicated liquid environments.

tions from a sulfoxy species, such as SO_2^{4-} (~168.6 eV), and an elemental sulfur or polysulfide (both of which might be expected to exhibit S 2p features near 163.4 eV). An alternative and our favored interpretation is that the initial surface product is $S_2O_3^{2-}$. This latter assignment would be consistent with the XPS-derived O:S and S (163.4 eV):S (168.6 eV) product stoichiometry of 1.3 ± 0.3 and 1.2 ± 0.2, respectively. The low O:S and high S:S ratio for thiosulfate might suggest that this species coexists with more reduced sulfur or polysulfide.

The S 2p reference spectrum of precipitated $Na_2S_2O_3$ on pyrite shows features at 168.6 and 162.5 eV. The surface product on FeS_2(100) formed after a 20-h exposure to H_2O vapor exhibits one of its features at 168.6 eV, but its second S 2p feature, which is presumably due to the terminal sulfur, is at 163.4 eV. This difference may be a result of the different bonding environments between the low oxidation state S species in the thiosulfate monolayer that forms during H_2O vapor treatment and the analogous S in the $Na_2S_2O_3$ salt. Specifically, the low oxidation S species in the thiosulfate monolayer formed during H_2O treatment is presumed to be coordinated directly to the pyrite surface, in contrast to the bulk $Na_2S_2O_3$.

A thiosulfate surface intermediate forming during pyrite oxidation is supported by prior aqueous based research (*9*, *25*). Our studies suggest that this oxidation surface product is in lowest concentration on the acid-washed surface and highest on the defective surface (high monosulfide concentration) after exposure to H_2O vapor. Formation of thiosulfate on the monosulfide impurity might suggest that S−S bond formation occurs to produce the thiosulfate at the expense of Fe−S bonding, which is presumably reduced due to concurrent oxidation of Fe. Our data suggest that after extended exposure to H_2O vapor (100 h) the thiosulfate coverts to primarily sulfate (XPS-determined O:S stoichiometry of 3.5 ± 0.3) on the highly defective surface, emphasizing its role as an intermediate in the oxidation process on FeS_2-(100).

Oxidation of FeS_2(100). The key experimental observations concerning the oxidation of pyrite are that H_2O vapor reacts primarily with nonstoichiometric regions of FeS_2(100), but when O_2 is present as a coreactant, oxidation of the disulfide group occurs.

With regard to H_2O alone, prior studies in our laboratory (*26*) suggest that H_2O binds specifically to defect sites (comprising ~10−15% of surface) that are at least in part sulfur anion vacancies. Dissociation of H_2O occurs on these sulfur-deficient sites but not on the disulfide site, which binds H_2O more weakly. The relatively strong binding of H_2O at the defect site as compared to the disulfide group of pyrite agrees with our experimental observation in the present study; namely, that the water-induced oxidation of FeS_2(100) is limited to the minority sulfur vacancy sites on pyrite. Whether activation of H_2O occurs on an exposed Fe^{2+} site of monosulfide or an Fe^{3+} defect site in close proximity cannot be unequivocally determined from our experimental results. The possibility of dissociation on the latter site, however, is a strong possibility and is supported by prior studies that have suggested that H_2O dissociates on Fe_2O_3 (*27*) and by well-known aqueous chemistry that shows that $Fe^{3+}(H_2O)_6$ has a significant acidity and is actually in equilibrium with H^+ and $Fe^{3+}(OH^-)(H_2O)_5$. Prior aqueous studies (*3*, *9*, *28*) and those presented here show that Fe^{3+} in solution acts as a strong oxidant of the pyrite surface.

While it is widely recognized that dissolved Fe^{3+} is a strong oxidant, we believe that *surface* Fe^{3+} sites play a key role in the oxidation of the disulfide group of FeS_2(100) in the H_2O/O_2 vapor environment. It is postulated that Fe^{3+} sites on stoichiometric regions of pyrite, created by charge transfer from Fe^{2+} species to O_2, provide active sites for H_2O dissociation. Prior research (*29*) has made a strong case for this charge-transfer step (i.e., $Fe^{2+} + O_2 \rightarrow Fe^{3+} + O_2^-$) being facilitated in regions where Fe^{2+} has nearest neighbor iron-(III) oxide sites. In short, the oxide product acts as a conduit for the electron transfer between Fe^{2+} and O_2. These prior results taken together with results derived from our study suggest that the nonstoichiometric regions of pyrite, which are readily oxidized even in the absence of O_2, form the Fe^{3+}−O surface phases that facilitate oxidation of surrounding stoichiometric pyrite surface in the H_2O/O_2 environment. Oxygen isotope studies by Reedy et al. (*30*) and Taylor et al. (*31*, *32*) indicate that the oxygen in sulfate resulting from abiotic pyrite oxidation is primarily derived from water, but some sulfate contains one or two oxygen atoms derived from O_2. This earlier result as well as our results indicate that water or an O-containing surface species derived from water is a key reactant in the creation of sulfur oxyanions. In essence, O_2 may act as an electron acceptor, creating adsorption sites for H_2O, but it is not essential for the conversion of S_2^{2-} to $S_nO_x^{2-}$. This statement agrees with prior aqueous research that shows that sulfur oxyanions also are formed if ferric iron replaces O_2 as the electron acceptor. While speculative, it is possible that an OH species or HO−OH (peroxide) species forms as a result of the dissociation of water on or near Fe^{3+} sites. More research is needed to address the fate of the O_2.

Our results are consistent with prior aqueous-based studies on pyrite oxidation, with regard to the effects of Fe^{3+} and O_2 on pyrite oxidation. Mechanistic implications from our work primarily apply to pyrite oxidation in the gaseous environment. One might speculate, however, that the aqueous oxidation model for pyrite should include surface confined Fe^{2+}−Fe^{3+} redox chemistry in the presence of O_2,

in addition to the solution and adsorbed phase $Fe^{2+} \rightarrow Fe^{3+}$ oxidation steps prominent in the models proposed by Singer and Stumm (*28*) and Moses and Herman (*8*), respectively. The results of this study also present an important implication for the development of techniques to abate acid mine drainage. The crucial initiating reaction step(s) may take place at defect sites on the pyrite surface. The role that additives such as phosphate and organic acids play may be to bind to these sites, thus inhibiting further reaction. Compounds that form strong bonds with Fe^{3+} deserve special attention.

Acknowledgments

D.R.S. and M.A.A.S. greatly appreciate support from the Department of Energy, Basic Energy Sciences from Grant DEFG0296ER14644 and DEFG029ER14633, respectively. J.M.G. thanks C. Guevremont for ideas used in design of the transfer chamber.

Literature Cited

(1) Evangelou, V. P. *Pyrite Oxidation and its Control*; CRC Press: Boca Raton, FL, 1995.
(2) See contributions in *Environmental Geochemistry of Sulfide Oxidation*; Alpers, C. N., Blowes, D. W., Eds.; American Chemical Society: Washington, DC, 1994; Vol. 550.
(3) Nordstrom, D. K.; Southam, G. In *Geomicrobiology: Interactions between microbes and minerals*; Banfield, J. F., Nealson, K. H., Eds.; Mineralogical Society of America: Wasington, DC, 1997; Vol. 35, Chapter 11, pp 361−390.
(4) Williamson, M. A.; Rimstidt, J. D. *Geochim. Cosmochim. Acta* **1994**, *58* (24), 5443−5454.
(5) Goldhaber, M. B. *Am. J. Sci.* **1983**, *283*, 193−217.
(6) Nicholson, R. V.; Gillham, R. W.; Reardon, E. J. *Geochim. Cosmochim. Acta* **1988**, *52*, 1077−1085.
(7) Nicholson, R. V.; Gillham, R. W.; Reardon, E. J. *Geochim. Cosmochim. Acta* **1990**, *54* (2), 395−402.
(8) Moses, C. O.; Herman, J. S. *Geochim. Cosmochim. Acta* **1991**, *55*, 471−482.
(9) Moses, C. O.; Nordstrom, D. K.; Herman, J. S.; Mills, A. L. *Geochim. Cosmochim. Acta* **1987**, *51* (6), 1561−1572.
(10) Bronold, M.; Tomm, Y.; Jaegermann, W. *Surf. Sci. Lett.* **1994**, *314*, L931−L936.
(11) Pettenkofer, C.; Jaegermann, W.; Bronold, M. *Ber. Bunsen-Ges. Phys. Chem.* **1991**, *95* (5), 560−565.
(12) Brion, D. *Appl. Surf. Sci.* **1980**, *5* (2), 133−152.
(13) Buckley, A. N.; Woods, R. *Appl. Surf. Sci.* **1987**, *27*, 437−452.
(14) Karthe, S.; Szargan, R.; Suoninen, E. *Appl. Surf. Sci.* **1993**, *72*, 157−170.
(15) Knipe, S. W.; Mycroft, J. R.; Pratt, A. R.; Nesbitt, H. W.; Bancroft, G. M. *Geochim. Cosmochim. Acta* **1995**, *59*, 1079−1090.
(16) Mycroft, J. R.; Bancroft, G. M.; McIntyre, N. S.; Lorimer, J. W.; Hill, I. R. *J. Electroanal. Chem.* **1990**, *292*, 139−152.
(17) Nesbitt, H. W.; Muir, I. J. *Geochim. Cosmochim. Acta* **1994**, *58* (21), 4667−4679.
(18) Schematic of design is available on the web at http://nimbus.ocis.temple.edu/~dstrongi/hghpres.html.
(19) Chaturvedi, S.; Katz, R.; Guevremont, J.; Schoonen, M. A. A.; Strongin, D. R. *Am. Mineral.* **1996**, *81*, 261−264.
(20) Bronold, M.; Büker, K.; Kubala, S.; Pettenkofer, C.; Tributsch, H. *Phys. Status Solidi A* **1993**, *135*, 231−243.
(21) Briggs, D.; Seah, M. P. *Practical Surface Analysis by Auger and X-ray Photoelectron Spectroscopy*; John Wiley & Sons: New York, 1983.
(22) Bebie, J.; Schoonen, M. A. A.; Fuhrmann, M.; Strongin, D. R. *Geochim. Cosmochim. Acta* **1998**, *62*, 633−642.
(23) Fukuda, Y.; Lancaster, F. M.; Honda, R.; Rabalais, J. W. *J. Chem. Phys.* **1978**, *69*, 3447.
(24) Furuyama, M.; Kishi, K.; Ikeda, S. *J. Electron Spectrosc. Relat. Phenom.* **1978**, *13*, 59−67.
(25) Steger, H. F.; Desjardins, L. E. *Chem. Geol.* **1978**, *23*, 225−237.
(26) Guevremont, J. M.; Strongin, D. R.; Schoonen, M. A. A. *Surf. Sci.* **1997**, *391*, 109−124.
(27) Kurtz, R. L.; Henrich, V. E. *Phys. Rev. B* **1987**, *36*, 3413−3421.
(28) Singer, P. C.; Stumm, W. *Science* **1970**, *167*, 1121−1123.
(29) The specifics of this process are elucidated in elegant experiments in the following reference: Eggleston, C. M.; Ehrhardt, J.; Stumm, W. *Am. Mineral.* **1996**, *81*, 1036−1056.
(30) Reedy, B. J.; Beattie, J. K.; Lowson, R. T. *Geochim. Cosmochim. Acta* **1991**, *55*, 1609−1614.
(31) Taylor, B. E.; Wheeler, M. C.; Nordstrom, D. K. *Nature* **1984**, *308*, 538−541.
(32) Taylor, B. E.; Wheeler, M. C.; Nordstrom, D. K. *Geochim. Cosmochim. Acta* **1984**, *48*, 2669−2678.

Received for review March 25, 1998. Revised manuscript received August 26, 1998. Accepted September 2, 1998.

ES980298H